

**Analytical analysis for additional ionization peaks of He induced by chirped xuv pulses**Yong-Kang Fang <sup>1</sup>, Lei Geng <sup>1</sup> and Liang-You Peng <sup>1,2,3,4,\*</sup><sup>1</sup>*State Key Laboratory for Mesoscopic Physics and Frontiers Science Center for Nano-Optoelectronics, School of Physics, Peking University, Beijing 100871, China*<sup>2</sup>*Collaborative Innovation Center of Quantum Matter, Beijing 100871, China*<sup>3</sup>*Collaborative Innovation Center of Extreme Optics, Shanxi University, Taiyuan 030006, China*<sup>4</sup>*Peking University Yangtze Delta Institute of Optoelectronics, Nantong, Jiangsu 226010, China*

(Received 28 October 2023; accepted 9 January 2024; published 29 January 2024)

When He is ionized by a chirped xuv pulse, additional peaks are identified in the joint energy spectra besides ordinary ionization peaks. Our results are based on the solution of the full-dimensional time-dependent Schrödinger equation of helium. Further numerical studies show that these additional structures are sensitive to both the pulse duration and the chirp parameter. To reveal the underlying mechanism, we have developed an analytical model based on the symmetric ionization assumption and the second-order time-dependent perturbation theory, which can qualitatively reproduce these additional structures. By systematic comparison studies, one can attribute the origin of these structures to the interference of two indistinguishable electrons and the diffraction in the time domain. In addition, we find that the interference effect is absent when one uses a negatively chirped laser pulse, while the diffraction in the time domain always persists.

DOI: [10.1103/PhysRevA.109.013113](https://doi.org/10.1103/PhysRevA.109.013113)**I. INTRODUCTION**

Owing to the availability of intense xuv sources from the high-order harmonic generation [1,2] and free-electron lasers [3–5], the ionization of atoms by absorption of a few photons has been experimentally accessible. As the simplest multielectron system, helium provides an ideal platform to study the role of the electron correlation. After several decades of investigations, the one-photon double ionization of helium has been well understood [6]. Three mechanisms have been proposed, i.e., the shake-off mechanism, the knock-out mechanism, and the quasifree mechanism from the quadrupole channel [7–10].

Recently, further efforts have been expended on the more complex two-photon double ionization (TPDI) of helium. In the long-pulse limit, the TPDI of helium is usually divided into two regimes, i.e., the nonsequential double ionization (NSDI) regime and the sequential double ionization (SDI) regime, depending on the photon energy. For the NSDI regime, TPDI can occur by simultaneously absorbing two photons with photon energy  $39.5 < \hbar\omega < 54.4$  eV, while for the SDI regime with photon energy  $\hbar\omega > 54.4$  eV TPDI can be regarded as a result of two sequential one-photon single ionizations (PSIs). Except for the discussion on the total cross section of TPDI [11–20], the differential spectra regarding the joint energy distribution and angular distribution also have been well studied [21,22]. In the SDI regime, the sequential peaks at energies  $\hbar\omega - I_{p1}$  and  $\hbar\omega - I_{p2}$  will appear in the energy spectra, with  $I_{p1} = 24.6$  eV and  $I_{p2} = 54.4$  eV being the first and second ionization potential of helium. If the photon energy is large enough, the shake-up channel can be

open and there will be more sequential peaks. As for the NSDI regime, the energy spectra will show a “U” shape. Besides, the angular distribution in the NSDI regime shows that the two electrons tend to be emitted through the back-to-back ejection mode. For the SDI regime, it is much more complex because the ejection mode of the two electrons depends on the energy sharing of two electrons [23–26]. Besides the studies of TPDI within the dipole approximation, there are several works to investigate the nondipole effects of the TPDI including the nondipole angular distribution parameters and the photon momentum transfer [27,28] by solving the full-dimensional time-dependent Schrödinger equation (TDSE) beyond the dipole approximation.

Although there are many theoretical studies for the TPDI of helium, very few works have been devoted to investigate the dynamic effects induced by a chirped xuv pulse [29–31]. Nevertheless, in Ref. [29], preliminary numerical results showed that the sequential peaks would change with the chirp parameter and unexpected additional structures between the sequential peaks were observed with a positive chirp parameter. However, the underlying mechanisms are elusive and how these structures will depend on the laser parameters was not discussed.

In this paper, we carry out a systematic investigation on the dynamic effects in the TPDI induced by a chirped xuv pulse. Based on a comparative studying of the results from TDSE and an analytical model, we find that the appearance and strength of additional structures are dependent on the sign and value of the chirp rate, as well as the photon energy and the pulse duration. These structures may be attributed to two different reasons, i.e., the interference of two indistinguishable electrons and the diffraction of the wave packets in the time domain. Our analytical model is based on the

\*liangyou.peng@pku.edu.cn

symmetric ionization assumption (SIA) and the second-order time-dependent perturbation theory (TDPT).

The rest of this paper is organized as follows. In Sec. II, we give a brief introduction to our TDSE and TDPT methods. Then we show how to develop the analytical method based on the SIA picture. In Sec. III, we present our results about these additional structures and show the mechanisms based on the SIA. In Sec. IV, we give a short summary. Unless otherwise stated, atomic units are used throughout this paper.

## II. THEORETICAL METHOD

One can assume that the chirped xuv pulse is polarized along the  $z$  direction, with its vector potential given by

$$\mathbf{A}(t, \xi) = A_0 f(t) \cos[\omega(t, \xi)t] \hat{\mathbf{e}}_z, \quad t \in \left[-\frac{T}{2}, \frac{T}{2}\right], \quad (1)$$

where  $\xi$ ,  $A_0$ , and  $T$  are the dimensionless chirp parameter, the peak amplitude, and the total pulse duration, respectively. In this paper, the laser intensity is fixed at  $10^{12}$  W/cm<sup>2</sup>. The case of  $\xi > 0$  ( $\xi < 0$ ) represents a positive (negative) chirp rate. We take the Gaussian envelope with

$$f(t) = \exp\left[-2 \ln 2 \frac{t^2}{\tau^2}\right], \quad (2)$$

where  $\tau$  is the full width at half maximum of the pulse, taken to be  $\frac{T}{4}$  throughout this paper. The instantaneous frequency  $\omega(t, \xi)$  is given by

$$\omega(t, \xi) = \omega_0 + 4 \ln 2 \frac{\xi t}{\tau^2}. \quad (3)$$

### A. Methods of TDSE and TDPT

The full-dimensional two-electron TDSE is solved within the dipole approximation in the length gauge. Details of the methodologies can be found in our previous work [27,32–34]. Here, we only give a brief introduction and specify the parameters used in the present paper. In the spherical coordinates, we employ the finite element discrete variable representation method to discretize the radial coordinates and the Lanczos propagator to evolve the two-electron wave function. The maximal numbers of the single angular momentum ( $l_{\max}$ ) and total angular momentum ( $L_{\max}$ ) are set to be 5 and 3, respectively. The average radial spacing is about 0.25 a.u. After the end of the pulse, the wave function is further propagated for a time period of 20 a.u. so that one can project it to the product of two Coulomb waves and obtain the differential momentum distribution of the two electrons  $P(\mathbf{k}_1, \mathbf{k}_2)$ , from which all other physical observables can be computed.

In order to understand the additional peaks observed in the results of TDSE, we also adapt the semianalytical model based on TDPT, in which the virtual sequential picture has been proposed to successfully describe many phenomena of double ionization of He [11,13,26,28,35–37]. According to the model, the joint energy distribution of two ionized electrons is given in the velocity gauge by

$$P(E_1, E_2) \propto |\sqrt{\sigma^{\text{He}}(E_1)\omega_{ai}}\sqrt{\sigma^{\text{He}^+}(E_2)\omega_{fa}}K(E_a) + \sqrt{\sigma^{\text{He}}(E_2)\omega_{bi}}\sqrt{\sigma^{\text{He}^+}(E_1)\omega_{fb}}K(E_b)|^2, \quad (4)$$

where  $E_1$  and  $E_2$  are the energies of two electrons,  $\sigma^{\text{He}}$  and  $\sigma^{\text{He}^+}$  are the PSI cross section of He and He<sup>+</sup>,  $\omega_{ai} = E_a - E_i$ ,  $\omega_{fa} = E_f - E_a$ ,  $\omega_{bi} = E_b - E_i$ ,  $\omega_{fb} = E_f - E_b$ ,  $E_i = -I_p = -I_{p1} - I_{p2}$ ,  $E_a = E_1 - I_{p2}$ ,  $E_b = E_2 - I_{p2}$ ,  $E_f = E_1 + E_2$ , and the function  $K(E_a)$  is given by

$$K(E_a) = \int_{-\infty}^{\infty} d\tau_1 A(\tau_1) e^{i\omega_{fa}\tau_1} \int_{-\infty}^{\tau_1} d\tau_2 A(\tau_2) e^{i\omega_{ai}\tau_2}, \quad (5)$$

where  $A(t)$  is the vector potential of the laser pulse. Replacing the subscript  $a$  by  $b$ , one immediately obtains a similar expression for  $K(E_b)$ . Please note that one can arrive at the same numerical result for  $P(E_1, E_2)$  in Eq. (4) if the length gauge is used, but with a slightly different expression.

For a Gaussian chirped pulse here, similar to Ref. [38] and starting from Eq. (5), one can carry out the integration of  $K(E_a)$  analytically by taking the rotation wave approximation and  $t_1 = \tau_1 + \tau_2$ ,  $t_2 = \tau_1 - \tau_2$  with Eq. (2), which gives

$$K(E_a) = \frac{A_0^2}{4} \int_{-T}^T dt_1 e^{i\frac{\Delta_r}{2}t_1} e^{-(1+2\xi i) \ln 2 \frac{t_1^2}{\tau^2}} \times \int_0^T dt_2 e^{i\frac{\Delta_r}{2}t_2} e^{-(1+2\xi i) \ln 2 \frac{t_2^2}{\tau^2}}, \quad (6)$$

in which  $\Delta_r = E_1 + E_2 + I_p - 2\omega_0$  and  $\Delta_i = -E_1 + E_2 + I_{p2} - I_{p1}$ . Later on, one will find that the SIA can reproduce the second line of Eq. (6), which accounts for the distribution of the energy difference between the two electrons. As for the first line of Eq. (6), it gives the distribution of two electrons' total energy, which will be a Gaussian distribution as well for the Gaussian laser pulse.

We note that, authors in Refs. [38,39] found that the chirped pulse can be considered as a pump-probe scheme due to the existence of the middle state, especially for  $2p\sigma_u$ . However, in our paper, such a middle state does not exist. Therefore, if we only consider it as a pump-probe scheme, we cannot reproduce the results of TDSE. In order to explain the results, we will instead develop the SIA picture below.

### B. Symmetric ionization assumption

Now, we proceed to show the illustration of the SIA of the two-photon double ionization induced by the chirped laser pulses. Taking the positive chirp as an example, the basic idea is shown in Fig. 1, in which the ionization time of the first and second electron is assumed to be symmetric with respect to the pulse center.

Based on the SIA picture, one can formally develop an analytical expression. Starting from the TDPT, we take  $K(E_a)$  as an example. In the rotation wave approximation,  $K(E_a)$  in Eq. (5) can be written as

$$K(E_a) \propto \int_{-\infty}^{\infty} d\tau_1 f(\tau_1) e^{-i(\omega_0\tau_1 + 4 \ln 2 \frac{\tau_1^2}{\tau^2} \xi)} e^{i\omega_{fa}\tau_1} \times \int_{-\infty}^{\tau_1} d\tau_2 f(\tau_2) e^{-i(\omega_0\tau_2 + 4 \ln 2 \frac{\tau_2^2}{\tau^2} \xi)} e^{i\omega_{ai}\tau_2}. \quad (7)$$

The symmetric ionization assumption means that  $\tau_1 + \tau_2 = 0$ , so the above expression can be simplified to

$$K(E_a) \propto \int_0^{\frac{T}{2}} dt f^2(t) e^{-i8 \ln 2 \frac{t^2}{\tau^2} \xi} e^{i(-E_- + I_{p2} - I_{p1})t}, \quad (8)$$

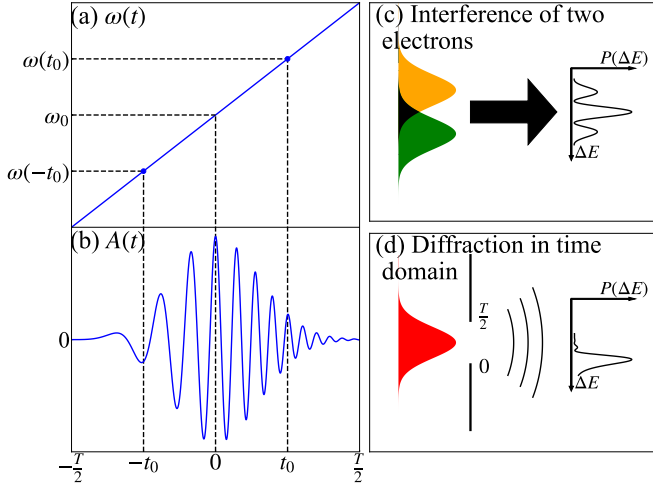


FIG. 1. Illustration of the SIA of TPDI induced by a positively chirped laser pulse. (a) The instantaneous frequency with a positive chirp rate. The ionization time of the first and second electrons is assumed to be symmetric relative to the pulse center (zero here). (b) The vector potential of the chirped pulse. (c) The interference of two indistinguishable electrons corresponding to Eq. (11). (d) The diffraction of the electron wave packet in the time domain without the consideration of the electron indistinguishability [see Eq. (12)].

with  $E_- = E_1 - E_2$  being the energy difference of two electrons. Taking  $t = t_2/2$ , one finds that Eq. (8) reproduces the second line of Eq. (6).

Besides, the assumption of  $\tau_1 + \tau_2 = 0$  can also be deduced from the on-shell ionization. For an unchirped pulse with a constant frequency  $\omega_0$ ,  $K(E_a)$  is given by

$$K(E_a) \propto \int_{-\infty}^{\infty} d\tau_1 f(\tau_1) e^{iE_{fa}\tau_1} \int_{-\infty}^{\tau_1} d\tau_2 f(\tau_2) e^{iE_{ai\omega}\tau_2}, \quad (9)$$

with  $E_{fa\omega} = \omega_{fa} - \omega_0$  and  $E_{ai\omega} = \omega_{ai} - \omega_0$ . The on-shell ionization requires that  $E_{fa\omega} + E_{ai\omega} = 0$ . Therefore, for a chirped laser pulse, starting from Eq. (7), by making use of the instantaneous frequency given in Eq. (3), the on-shell ionization condition turns out to be

$$\omega_{fa} - \left( \omega_0 + 4 \ln 2 \frac{\tau_1}{\tau^2} \xi \right) + \omega_{ai} - \left( \omega_0 + 4 \ln 2 \frac{\tau_2}{\tau^2} \xi \right) = 0,$$

which can be reduced to

$$4 \ln 2 \frac{\xi}{\tau^2} (\tau_1 + \tau_2) = E_1 + E_2 + I_p - 2\omega_0, \quad (10)$$

which means  $\tau_1 + \tau_2 = 0$  if  $E_{\text{tot}} = E_1 + E_2 = 2\omega_0 - I_p$ .

With the same arguments, one can get a similar expression for  $K(E_b)$ . Finally, one gets the distribution of  $P(E_-)$  at  $E_{\text{tot}} = 2\omega_0 - I_p$  with SIA by

$$\begin{aligned} P(E_-)|_{E_{\text{tot}}=2\omega_0-I_p} &= P(E_-, E_{\text{tot}} = 2\omega_0 - I_p) \\ &\propto P(E_1, E_2)|_{E_1+E_2=2\omega_0-I_p} \\ &\propto |Q(-E_-) + Q(E_-)|^2, \end{aligned} \quad (11)$$

where the function  $Q(E)$  is given by

$$Q(E) = \int_0^{\frac{\tau}{2}} dt f^2(t) e^{-i8 \ln 2 \frac{\tau^2}{\tau^2} \xi} e^{i(E+I_{p2}-I_{p1})t}. \quad (12)$$

For a chirped Gaussian pulse with envelope Eq. (2), the expression for  $Q(E)$  can be further reduced to

$$Q(E) \propto e^{-(1-2\xi i) \frac{T^2(E+I_{p2}-I_{p1})^2}{256(1+4\xi^2)\ln^2}} [\text{erf}(z_2) - \text{erf}(z_1)], \quad (13)$$

in which  $\text{erf}(z)$  is the error function, whose arguments  $z_1$  and  $z_2$  are respectively given by

$$\begin{aligned} z_1 &= e^{i(\frac{\pi}{4} - \frac{\theta}{2})} \frac{T(E + I_{p2} - I_{p1})}{16\sqrt{1 + 4\xi^2}\sqrt{\ln 2}}, \\ z_2 &= z_1 + z_0, \\ z_0 &= e^{i(\frac{5\pi}{4} + \frac{\theta}{2})} 4\sqrt{\ln 2}\sqrt{1 + 4\xi^2}, \end{aligned} \quad (14)$$

where  $\theta$  equals to  $\text{Arg}(2\xi - i) \in (-\pi, 0)$ .

Now, we can give a simple discussion of the structure observed in the distribution of  $P(E_-)$ , which is illustrated in Figs. 1(c) and 1(d). The first origin of the structure is the interference of two indistinguishable electrons due to the overlap of the electron wave packets through the first and second ionization. Note that it should only exist with a positive chirp. For a negative chirp, it is impossible for the two wave packets to overlap each other.

The second origin of the structure can be considered as the diffraction of the wave packet in the time domain. For a short pulse duration, such effects may be hidden by the interference effects of the two indistinguishable electrons. However, it will be obvious with a sufficiently long pulse. Without the consideration of interference effects of the two indistinguishable electrons, one can have a better look at Eq. (12). Different from the traditional single slit diffraction where the strength is uniform with a linear phase, here one notices that the strength will decrease with time ( $t \geq 0$ ) and the chirp induces a quadratic phase. It can result in the oscillatory structure which will be shown below. Finally, it is important to point out that, unlike the indistinguishable interference effect, the diffraction effect will also exist for a negative chirp rate. According to Eqs. (11) and (12), one finds that both the indistinguishable interference effect and the diffraction effect only depend on the pulse duration and the chirp parameter.

### III. RESULTS AND DISCUSSIONS

In this section, we will present our main results and discussions based on the TDSE and models shown in the last section.

In Fig. 2, for  $\omega_0 = 52.7$  eV and  $\xi = 1.75$ , we show the joint energy distributions of two electrons calculated by TDSE and TDPT, as well as the distributions of  $P(E_-)$  at  $E_{\text{tot}} = 2\omega_0 - I_p$  from TDSE, TDPT, and SIA. As one can see, the results of TDSE and TDPT agree with each other quite well. From Fig. 2(c), one can clearly observe the additional peak between the two sequential peaks. Different from that previously observed in Refs. [29,30], here the additional peak is much stronger than the usual sequential peaks for the pulse duration of 1 fs. If one increases the pulse duration to 2 fs, the additional single peak will split into multiple peaks, as shown in Fig. 2(f).

In Figs. 2(a) and 2(d) [as well as Figs. 2(b) and 2(e)], one may notice that the maximum in the distribution of  $P(E_1, E_2)$

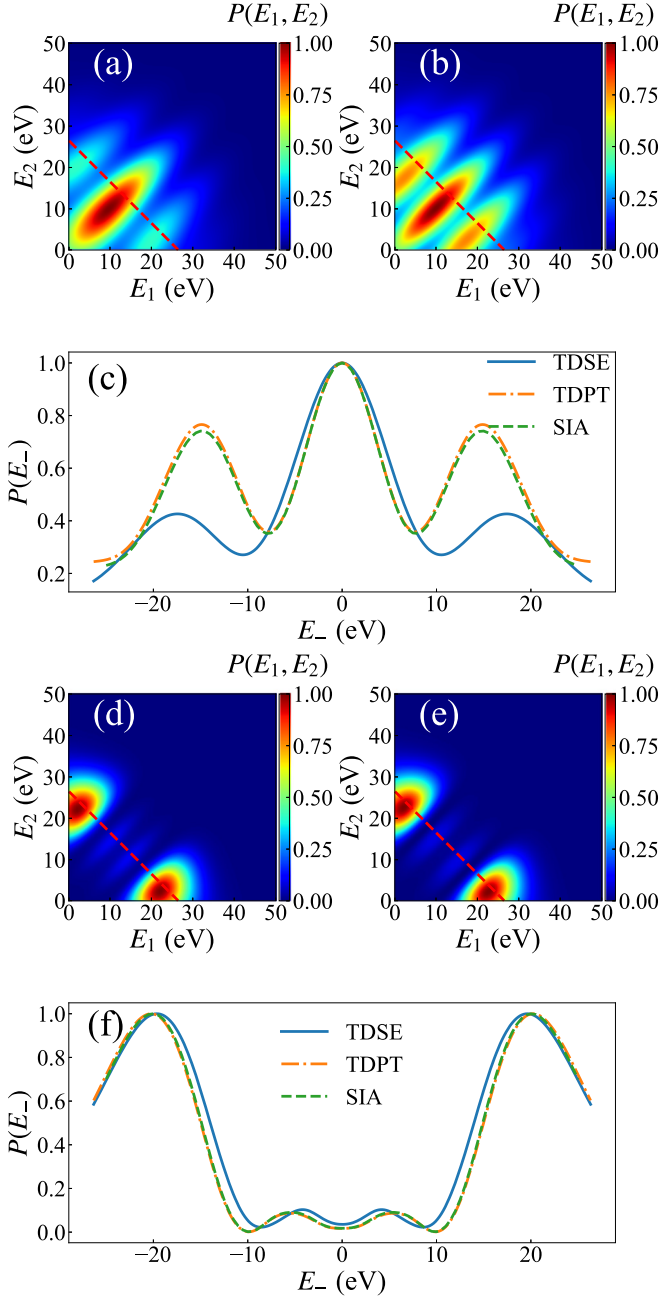


FIG. 2. The results for  $\omega_0 = 52.7$  eV and  $\xi = 1.75$  at two different pulse durations of 1 fs (a)–(c) and 2 fs (d)–(f). (a), (d) The joint energy distributions of two electrons from TDSE. (b), (e) The joint energy distributions of two electrons from TDPT. (c), (f) The distributions of  $P(E_-)$  at  $E_{\text{tot}} = 2\omega_0 - I_p$ , which is indicated by red dashed lines in (a), (b), (d), and (e). The blue solid lines, orange dash-dotted lines, and green dashed lines are the results of TDSE, TDPT, and SIA, respectively. All the distributions are normalized by the maximum.

deviates from the red dashed lines predicted by  $E_1 + E_2 = 2\omega_0 - I_p$  if one assumes the independence of cross section in energy. However, for our purpose of discussion for  $P(E_-)$ , it is sufficient to consider the distribution of  $P(E_-)$  at  $E_{\text{tot}} = 2\omega_0 - I_p$ . The conclusions will not change if one examines it at other values of the total energy.

As shown in Fig. 2(c), one finds that results of  $P(E_-)$  from TDPT and SIA are almost identical, although their relative ratios between the additional and the sequential peaks from both models significantly differ from the accurate results of TDSE where one takes the electron correlation into full consideration. For a longer pulse of 2 fs, as shown in Fig. 2(f), the distributions of  $P(E_-)$  from TDSE, TDPT, and SIA agree with each other much better as the electron correlation becomes less important.

From the above discussions, although the electron correlation can play some role, the main structures of additional peaks observed in  $P(E_-)$  are consistent among the results of TDSE, TDPT, and SIA. In order to uncover the mechanism behind the structure, i.e., the interference effect and the diffraction effect, we show the results of SIA and the part of  $|Q(-E_-)|^2$  and  $|Q(E_-)|^2$  in Fig. 3. In addition, we also show the incoherent distribution of  $P_{\text{IC}}(E_-) \propto |Q(-E_-)|^2 + |Q(E_-)|^2$ . Besides the ordinary sequential peaks, one finds that in the distribution of  $|Q(-E_-)|^2$  and  $|Q(E_-)|^2$ , there will be additional peaks which do not exist with an unchirped laser pulse, which will be called “chirped peaks” below.

The formation of the chirped peaks originates from the diffraction effect. Besides, the indistinguishability of the two electrons leads to the coherent superposition of the  $Q(-E_-)$  and  $Q(E_-)$ , which finally gives the SIA results of  $P(E_-)$ . Comparing with these results at a fixed chirp parameter, one finds that the difference between the distributions of the coherent and the incoherent summation becomes smaller and smaller when the laser pulse duration gets longer. Such a behavior is reasonable because by increasing the pulse duration, the frequency bandwidth will decrease. Therefore, the overlapping of the  $Q(-E_-)$  and  $Q(E_-)$  becomes smaller.

The indistinguishable interference effect will be quite important and even hide the chirped peaks when the pulse duration is short. In addition, one can infer that for a fixed pulse duration the interference effect will be quite important for a larger chirp rate.

For a better understanding of the diffraction effect, we proceed to examine the chirped peaks without the consideration of the interference effect. This can be done by only looking at the distribution of  $|Q(E)|^2$ , as shown in Fig. 4 for various chirp rates. Clearly, one finds that the distributions of the positive and negative chirp rates are symmetric about the orange vertical solid line. According to Eq. (12), one has

$$Q(E) = \int_0^{T/2} dt f^2(t) e^{i\phi(t)}, \quad (15)$$

$$\phi(t) = -8 \ln 2 \frac{t^2}{\tau^2} \xi + (E + I_{p2} - I_{p1})t, \quad (16)$$

which tells us that the chirped peaks come from the diffraction in the time domain, but the phase is quadratically dependent on  $t$  and the strength is decreasing with  $t$  ( $t \geq 0$ ). It is well known that, for a uniform strength in the case of a linear phase, the maxima and minima can be predicted by  $\int_0^T dt e^{it} = -i(e^{iT} - 1)$ . Specifically, it gives the maxima for  $T = (2n - 1)\pi$  and the minima for  $T = 2n\pi$ , with  $n = 1, 2, 3, \dots$ . For the present case of a quadratic phase and a

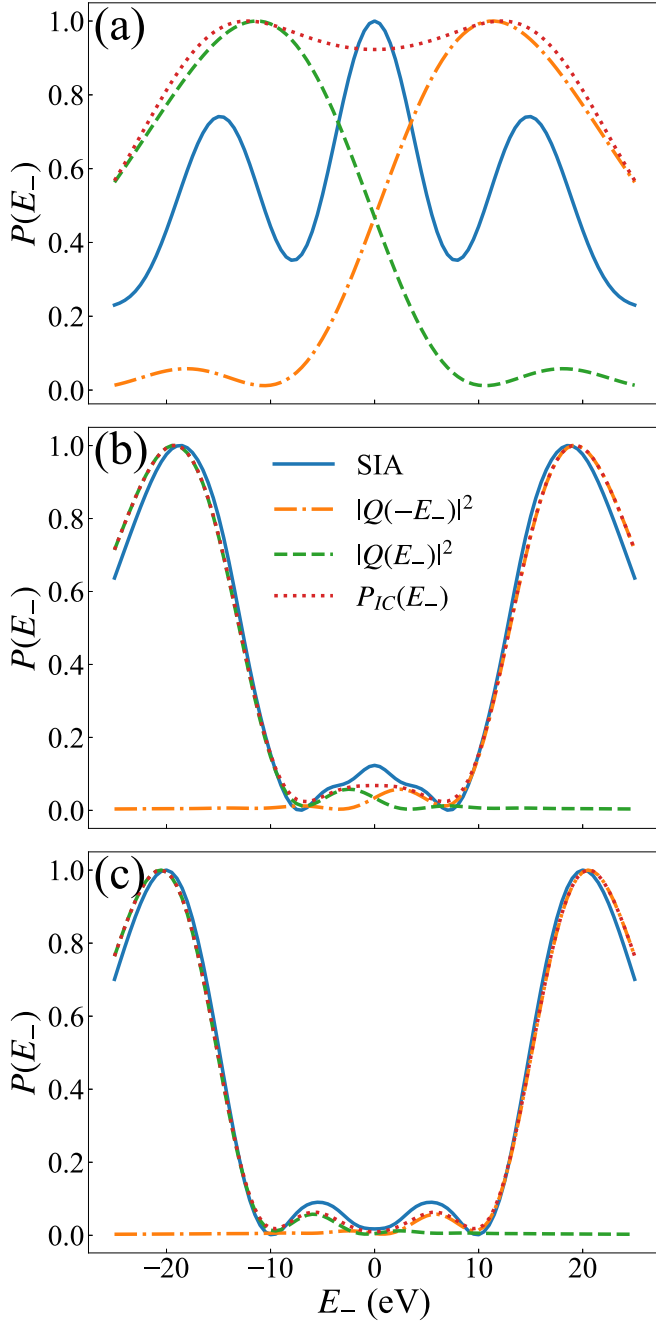


FIG. 3. The distributions of  $P(E_-)$  from SIA with  $\omega_0 = 52.7$  eV and  $\xi = 1.75$  at three different pulse durations of (a) 1 fs, (b) 1.75 fs, and (c) 2 fs. The results from Eq. (11) are shown in blue solid lines while the results of the part of  $|Q(-E_-)|^2$  and  $|Q(E_-)|^2$  are shown in orange dash-dotted lines and green dashed lines. The incoherent distributions of  $P_{IC}(E_-) \propto |Q(-E_-)|^2 + |Q(E_-)|^2$  are shown in red dotted lines. All the distributions are normalized by the maximum.

decreasing strength, we suppose at  $t_0$  the quadratic phase  $\phi(t)$  acquires its extreme value, i.e.,  $\frac{\partial \phi(t)}{\partial t}|_{t=t_0} = 0$ . One further supposes that  $\phi(t)$  can be approximately considered as linear within  $t \in (0, t_0)$ . Then, we can assume that the strength is uniform within  $t \in (0, t_0)$  and becomes zero for  $t > t_0$ . The maxima and minima can then be given by  $\phi(t_0) = (2n - 1)\pi$  and  $\phi(t_0) = 2n\pi$  with  $n = 1, 2, 3, \dots$ . Therefore, by using

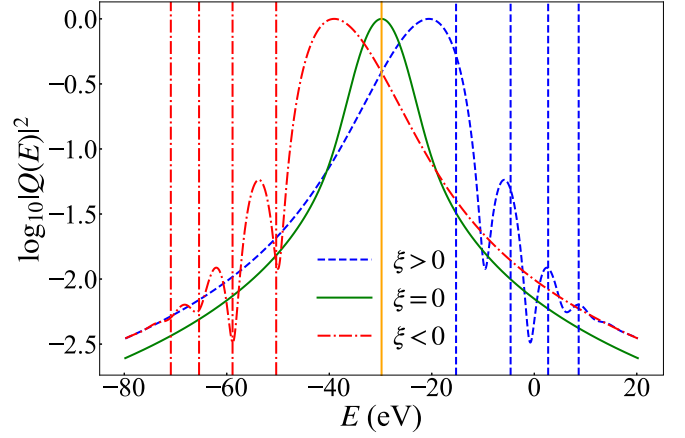


FIG. 4. The distributions of  $|Q(E)|^2$  for a pulse duration of  $T = 2$  fs at a positive chirp ( $\xi = 1.75$ , blue dashed line), a negative chirp ( $\xi = -1.75$ , red dash-dotted line), and a zero chirp (green solid line). All the distributions are normalized by the maximum. The orange vertical solid line represents the position of  $I_{p1} - I_{p2}$ . For clarity, we only show the maxima corresponding to Eq. (17) with blue dashed vertical lines for the positive chirp and the minima corresponding to Eq. (18) with red dash-dotted vertical lines for the negative chirp.

Eq. (16), we can estimate the positions of the maxima and minima by

$$E_{\max} = \begin{cases} I_{p1} - I_{p2} + \sqrt{\frac{32 \ln 2(2n-1)\xi}{\tau^2}}, & \xi > 0, \\ I_{p1} - I_{p2} - \sqrt{-\frac{32 \ln 2(2n-1)\xi}{\tau^2}}, & \xi < 0, \end{cases} \quad (17)$$

$$E_{\min} = \begin{cases} I_{p1} - I_{p2} + \sqrt{\frac{32 \ln 2(2n\xi)}{\tau^2}}, & \xi > 0, \\ I_{p1} - I_{p2} - \sqrt{-\frac{32 \ln 2(2n\xi)}{\tau^2}}, & \xi < 0, \end{cases} \quad (18)$$

with  $n = 1, 2, 3, \dots$ . For clarity, we only show the maxima with blue dashed vertical lines for the positive chirp and the minima with red dash-dotted vertical lines for the negative chirp in Fig. 4. One finds the predictions are in reasonably good agreement with the actual results. According to Eqs. (17) and (18), one finds the maxima and minima positions only depend on the pulse duration and the chirp rate. Further, one can infer that similar results can be achieved by increasing the pulse duration or decreasing the chirp parameter.

Although the additional peaks due to the diffraction and the indistinguishable interference effects only depend on the pulse duration and chirp parameter, the photon energy  $\omega_0$  will influence whether the complete structures can be resolved or not. For example, we have already shown the results for  $\omega = 52.7$  eV, which belongs to the NSDI regime. For the SDI regime, all the main features will persist and the results of the model match those of TDSE more closely. However, for the deep NSDI regime, e.g.,  $\omega = 42$  eV, the electron correlation will be quite important and drastically change the interference structures. We find that neither the TDPT nor the SIA can reproduce the TDSE results (not shown here).

Finally, we have mentioned the indistinguishable interference effect only exists for a positive chirp while the diffraction effect can also be found for a negative chirp in principle. Nevertheless, one cannot find the diffraction effect with a negative chirp for photon energy of  $\omega = 52.7$  eV because

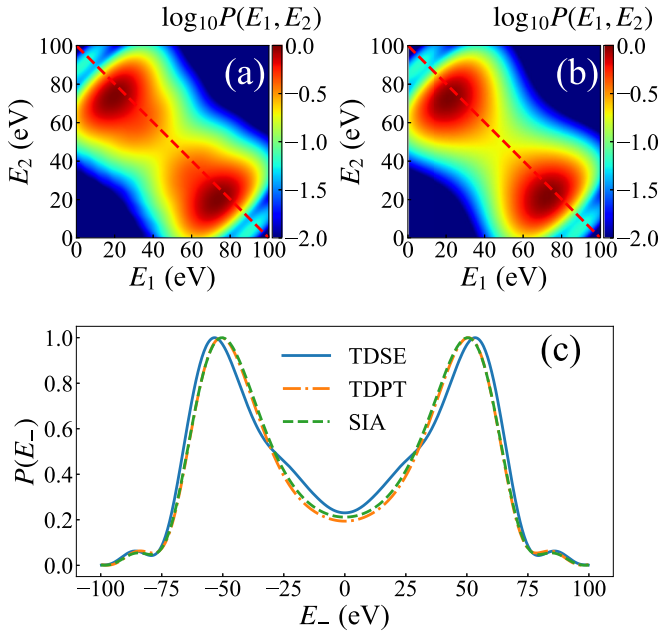


FIG. 5. Similar to Fig. 2, but for  $\omega_0 = 90$  eV,  $\xi = -2$ , and  $T = 20T_c$  with  $T_c = \frac{2\pi}{\omega_0}$ . All the distributions are normalized by the maximum. To better show the structure due to the negative chirp, the joint energy distributions in (a) and (b) are shown for  $\log_{10} P(E_1, E_2)$ . The distributions of  $P(E_-)$  are shown in (c). Note that, outside the ordinary sequential peaks, the peaks induced by the diffraction effect do appear.

the energy difference  $E_-$  between two electrons is not large enough. Therefore, in Fig. 5, we show the distributions with  $\omega_0 = 90$  eV,  $\xi = -2$ , and  $T = 20T_c$  with  $T_c = \frac{2\pi}{\omega_0}$ . It is clear that in the joint energy distributions of both TDSE and TDPT, outside the ordinary sequential peaks, the peaks induced by the diffraction effect do appear. The distributions of  $P(E_-)$  from TDSE, TDPT, and SIA agree with each other, which confirms the above discussions.

One may notice that there seem to be additional signatures between the ordinary sequential peaks for the results of TDSE. We point out that it should belong to the shake-up channel [21], i.e., for the middle state,  $\text{He}^+$  can be in the excited state ( $n = 2, 3, \dots$ ). The shift of the sequential peaks from the ordinary channel ( $n = 1$ ) is opposite to the sequential peaks from the shake-up channel ( $n = 2, 3, \dots$ ) with a chirped laser pulse.

#### IV. CONCLUSION

In summary, we have systematically examined the additional ionization peaks between the usual sequential peaks in the TPDI process of helium by a chirped laser pulse. Depending on the laser parameters, it can be much stronger than the usual sequential peaks or split into multiple peaks. Starting from the TDPT model, we have developed the SIA picture to uncover the mechanism behind these structures. It is found that the interference effect between the two indistinguishable electrons and the diffraction effect in the time domain are responsible for the formation of these structures. The interference effect should only exist with a positive chirp. As for the diffraction effect, one can successfully predict the peak and valley positions. It should also exist with a negative chirp. Further, it is found that the interference and diffraction effects only depend on the pulse duration and the chirp parameter, although the photon energy will influence whether the complete structure can be resolved or not in the spectra. Finally, according to the SIA model, the target plays little role, and it is believed that similar results can be derived for other noble gases which have a larger cross section than helium and will be easier to observe experimentally.

#### ACKNOWLEDGMENT

This work is supported by National Natural Science Foundation of China Grants No. 92250303 and No. 12234002.

- 
- [1] M. Hentschel, R. Kienberger, C. Spielmann, G. Reider, N. Milosevic, T. Brabec, P. Corkum, U. Heinzmann, M. Drescher, and F. Krausz, Attosecond metrology, *Nature (London)* **414**, 509 (2001).
- [2] P. M. Paul, E. S. Toma, P. Breger, G. Mullot, F. Augé, P. Balcou, H. G. Muller, and P. Agostini, Observation of a train of attosecond pulses from high harmonic generation, *Science* **292**, 1689 (2001).
- [3] P. Emma, R. Akre, J. Arthur, R. Bionta, C. Bostedt, J. Bozek, A. Brachmann, P. Bucksbaum, R. Coffee, F. J. Decker, Y. Ding, D. Dowell, S. Edstrom, A. Fisher, J. Frisch, S. Gilevich, J. Hastings, G. Hays, P. Hering, Z. Huang *et al.*, First lasing and operation of an angstrom-wavelength free-electron laser, *Nat. Photon.* **4**, 641 (2010).
- [4] B. W. J. McNeil and N. R. Thompson, X-ray free-electron lasers, *Nat. Photon.* **4**, 814 (2010).
- [5] T. Ishikawa, H. Aoyagi, T. Asaka, Y. Asano, N. Azumi, T. Bizen, H. Ego, K. Fukami, T. Fukui, Y. Furukawa, S. Goto, H. Hanaki, T. Hara, T. Hasegawa, T. Hatsui, A. Higashiya, T. Hirono, N. Hosoda, M. Ishii, T. Inagaki *et al.*, A compact x-ray free-electron laser emitting in the sub-angstrom region, *Nat. Photon.* **6**, 540 (2012).
- [6] J. S. Briggs and V. Schmidt, Differential cross sections for photo-double-ionization of the helium atom, *J. Phys. B* **33**, R1 (2000).
- [7] T. Schneider, P. L. Chocian, and J.-M. Rost, Separation and identification of dominant mechanisms in double photoionization, *Phys. Rev. Lett.* **89**, 073002 (2002).
- [8] J. Andersson, S. Zagorodskikh, A. H. Roos, O. Talaee, R. J. Squibb, D. Koulentianos, M. Wallner, V. Zhaunerchyk, R. Singh, J. H. D. Eland, J. M. Rost, and R. Feifel, Parametrization of energy sharing distributions in direct double photoionization of He, *Sci. Rep.* **9**, 17883 (2019).
- [9] S. Grundmann, F. Trinter, A. W. Bray, S. Eckart, J. Rist, G. Kastirke, D. Metz, S. Klumpp, J. Viehhaus, L. P. H. Schmidt, J. B. Williams, R. Dörner, T. Jahnke, M. S. Schöffler, and A. S. Kheifets, Separating dipole and quadrupole contributions to

- single-photon double ionization, *Phys. Rev. Lett.* **121**, 173003 (2018).
- [10] M. Y. Amusia, E. G. Drukarev, V. G. Gorshkov, and M. O. Kazachkov, Two-electron photoionization of helium, *J. Phys. B* **8**, 1248 (1975).
- [11] A. Palacios, T. N. Rescigno, and C. W. McCurdy, Time-dependent treatment of two-photon resonant single and double ionization of helium by ultrashort laser pulses, *Phys. Rev. A* **79**, 033402 (2009).
- [12] J. Feist, S. Nagele, R. Pazourek, E. Persson, B. I. Schneider, L. A. Collins, and J. Burgdörfer, Nonsequential two-photon double ionization of helium, *Phys. Rev. A* **77**, 043420 (2008).
- [13] D. A. Horner, F. Morales, T. N. Rescigno, F. Martín, and C. W. McCurdy, Two-photon double ionization of helium above and below the threshold for sequential ionization, *Phys. Rev. A* **76**, 030701(R) (2007).
- [14] L. A. A. Nikolopoulos and P. Lambropoulos, Time-dependent theory of double ionization of helium under XUV radiation, *J. Phys. B* **40**, 1347 (2007).
- [15] I. A. Ivanov and A. S. Kheifets, Two-photon double ionization of helium in the region of photon energies 42–50 eV, *Phys. Rev. A* **75**, 033411 (2007).
- [16] E. Fomouuo, G. L. Kamta, G. Edah, and B. Piraux, Theory of multiphoton single and double ionization of two-electron atomic systems driven by short-wavelength electric fields: An ab initio treatment, *Phys. Rev. A* **74**, 063409 (2006).
- [17] A. A. Sorokin, M. Wellhöfer, S. V. Bobashev, K. Tiedtke, and M. Richter, X-ray-laser interaction with matter and the role of multiphoton ionization: Free-electron-laser studies on neon and helium, *Phys. Rev. A* **75**, 051402(R) (2007).
- [18] H. Hasegawa, E. J. Takahashi, Y. Nabekawa, K. L. Ishikawa, and K. Midorikawa, Multiphoton ionization of He by using intense high-order harmonics in the soft-x-ray region, *Phys. Rev. A* **71**, 023407 (2005).
- [19] P. Antoine, E. Fomouuo, B. Piraux, T. Shimizu, H. Hasegawa, Y. Nabekawa, and K. Midorikawa, Two-photon double ionization of helium: An experimental lower bound of the total cross section, *Phys. Rev. A* **78**, 023415 (2008).
- [20] H. Shimada, K. Komatsu, W. Komatsubara, T. Mizuno, S. Miyake, S. Minemoto, H. Sakai, T. Majima, S. Owada, T. Togashi, M. Yabashi, and A. Yagishita, Two- and three-photon double ionization of helium by soft x-ray free-electron laser pulses, *J. Phys. B* **52**, 065602 (2019).
- [21] R. Pazourek, J. Feist, S. Nagele, E. Persson, B. I. Schneider, L. A. Collins, and J. Burgdörfer, Universal features in sequential and nonsequential two-photon double ionization of helium, *Phys. Rev. A* **83**, 053418 (2011).
- [22] J. Feist, R. Pazourek, S. Nagele, E. Persson, B. I. Schneider, L. A. Collins, and J. Burgdörfer, Electron correlation in two-photon double ionization of helium from attosecond to XFEL pulses, *J. Phys. B* **42**, 134014 (2009).
- [23] S. Laulan and H. Bachau, Correlation effects in two-photon single and double ionization of helium, *Phys. Rev. A* **68**, 013409 (2003).
- [24] J. Feist, S. Nagele, R. Pazourek, E. Persson, B. I. Schneider, L. A. Collins, and J. Burgdörfer, Probing electron correlation via attosecond xuv pulses in the two-photon double ionization of helium, *Phys. Rev. Lett.* **103**, 063002 (2009).
- [25] E. Fomouuo, A. Hamido, P. Antoine, B. Piraux, H. Bachau, and R. Shakeshaft, Time-dependent analysis of the mechanism for two-photon double escape in helium: from very long to attosecond time scales, *J. Phys. B* **43**, 091001 (2010).
- [26] W.-C. Jiang, J.-Y. Shan, Q. Gong, and L.-Y. Peng, Virtual sequential picture for nonsequential two-photon double ionization of helium, *Phys. Rev. Lett.* **115**, 153002 (2015).
- [27] Y.-K. Fang, H. Liang, W.-C. Jiang, and L.-Y. Peng, Angular distribution parameters in two-photon double ionization of helium beyond the dipole approximation, *Phys. Rev. A* **105**, 013104 (2022).
- [28] Y.-K. Fang, H. Liang, W.-C. Jiang, and L.-Y. Peng, Nonlinear scaling in photon momentum transfer caused by two-electron effects, *Phys. Rev. A* **106**, 023104 (2022).
- [29] T.-G. Lee, M. S. Pindzola, and F. Robicheaux, Energy and angular differential probabilities for photoionization of he using chirped attosecond soft-x-ray pulses, *Phys. Rev. A* **79**, 053420 (2009).
- [30] S. Barmaki, P. Lanteigne, and S. Laulan, Control of two-photon double ionization of helium with intense chirped attosecond laser pulses, *Phys. Rev. A* **89**, 063406 (2014).
- [31] Y. Tong, W.-C. Jiang, P. Wu, and L.-Y. Peng, Two-photon double ionization of helium by chirped few-cycle attosecond pulses: From nonsequential to sequential regime, *Chin. Phys. B* **25**, 073202 (2016).
- [32] Z. Zhang, L.-Y. Peng, M.-H. Xu, A. F. Starace, T. Morishita, and Q. Gong, Two-photon double ionization of helium: Evolution of the joint angular distribution with photon energy and two-electron energy sharing, *Phys. Rev. A* **84**, 043409 (2011).
- [33] W.-C. Jiang, L.-Y. Peng, W.-H. Xiong, and Q. Gong, Comparison study of electron correlation in one-photon and two-photon double ionization of helium, *Phys. Rev. A* **88**, 023410 (2013).
- [34] W.-C. Jiang, S.-G. Chen, L.-Y. Peng, and J. Burgdörfer, Two-electron interference in strong-field ionization of he by a short intense extreme ultraviolet laser pulse, *Phys. Rev. Lett.* **124**, 043203 (2020).
- [35] W.-C. Jiang, W.-H. Xiong, T.-S. Zhu, L.-Y. Peng, and Q. Gong, Double ionization of he by time-delayed attosecond pulses, *J. Phys. B* **47**, 091001 (2014).
- [36] A. Palacios, T. N. Rescigno, and C. W. McCurdy, Two-electron time-delay interference in atomic double ionization by attosecond pulses, *Phys. Rev. Lett.* **103**, 253001 (2009).
- [37] D. A. Horner, C. W. McCurdy, and T. N. Rescigno, Triple differential cross sections and nuclear recoil in two-photon double ionization of helium, *Phys. Rev. A* **78**, 043416 (2008).
- [38] D. Jelovina, J. Feist, F. Martín, and A. Palacios, A pump–probe scheme with a single chirped pulse to image electron and nuclear dynamics in molecules, *New J. Phys.* **20**, 123004 (2018).
- [39] D. Jelovina, J. Feist, F. Martín, and A. Palacios, Imaging ultrafast molecular wave packets with a single chirped uv pulse, *Phys. Rev. A* **95**, 043424 (2017).